AMERICAN SOCIETY FOR MICROBIOLOGY | Molecular and Cellular Biology®

RESEARCH ARTICLE

TAX1BP1 Restrains Virus-Induced Apoptosis by Facilitating Itch-Mediated Degradation of the Mitochondrial Adaptor MAVS

Young Bong Choi,[a] Noula Shembade,[b] Kislay Parvatiyar,[b]* Siddharth Balachandran,[c] Edward William Harhaj[a]

Department of Oncology, Sidney Kimmel Comprehensive Cancer Center, Johns Hopkins School of Medicine, Baltimore, Maryland, USA[a]; Department of Microbiology and Immunology, Sylvester Comprehensive Cancer Center, The University of Miami, Miller School of Medicine, Miami, Florida, USA[b]; Blood Cell Development and Function Program, Fox Chase Cancer Center, Philadelphia, Pennsylvania, USA[c]

ABSTRACT The host response to RNA virus infection consists of an intrinsic innate immune response and the induction of apoptosis as mechanisms to restrict viral replication. The mitochondrial adaptor molecule MAVS plays critical roles in coordinating both virus-induced type I interferon production and apoptosis; however, the regulation of MAVS-mediated apoptosis is poorly understood. Here, we show that the adaptor protein TAX1BP1 functions as a negative regulator of virus-induced apoptosis. TAX1BP1-deficient cells are highly sensitive to apoptosis in response to infection with the RNA viruses vesicular stomatitis virus and Sendai virus and to transfection with poly(I·C). TAX1BP1 undergoes degradation during RNA virus infection, and loss of TAX1BP1 is associated with apoptotic cell death. TAX1BP1 deficiency augments virus-induced activation of proapoptotic c-Jun N-terminal kinase (JNK) signaling. Virus infection promotes the mitochondrial localization of TAX1BP1 and concomitant interaction with the mitochondrial adaptor MAVS. TAX1BP1 recruits the E3 ligase Itch to MAVS to trigger its ubiquitination and degradation, and loss of TAX1BP1 or Itch results in increased MAVS protein expression. Together, these results indicate that TAX1BP1 functions as an adaptor molecule for Itch to target MAVS during RNA virus infection and thus restrict virus-induced apoptosis.

KEYWORDS Itch, MAVS, RNA viruses, TAX1BP1, innate immunity, ubiquitination

Received 19 July 2016 **Returned for modification** 4 August 2016 **Accepted** 4 October 2016

Accepted manuscript posted online 10 October 2016

Citation Choi YB, Shembade N, Parvatiyar K, Balachandran S, Harhaj EW. 2017. TAX1BP1 restrains virus-induced apoptosis by facilitating Itch-mediated degradation of the mitochondrial adaptor MAVS. Mol Cell Biol 37:e00422-16. https://doi.org/10.1128/MCB.00422-16.

Address correspondence to Young Bong Choi, ychoi15@jhmi.edu, or Edward William Harhaj, eharhaj1@jhmi.edu.

* Present address: Kislay Parvatiyar, Department of Microbiology, Immunology and Molecular Genetics, University of California at Los Angeles, Los Angeles, California, USA.

Virus infection triggers an intrinsic innate immune response that culminates in the production of proinflammatory cytokines (e.g., interleukin-1β [IL-1β], tumor necrosis factor [TNF], and type I interferons [IFNs; predominantly alpha interferon and beta interferon]). Activation of an innate immune antiviral response relies on a class of specialized pattern recognition receptors (PRRs) that detect conserved molecular features of viruses and other pathogens. The cytoplasmic RNA helicases RIG-I and MDA5 are key antiviral PRRs that recognize nucleic acids derived from RNA viruses and trigger downstream signaling dependent on the mitochondrial adaptor MAVS (also known as IPS-1, VISA, and Cardif), leading to activation of NF-κB and IFN regulatory factor 3 (IRF3) transcription factors that upregulate expression of proinflammatory cytokines and type I IFNs, respectively (1, 2). MAVS recruits E3 ubiquitin ligase TRAF proteins (TRAF2, TRAF3, TRAF5, and TRAF6) to conjugate lysine 63 (K63)-linked polyubiquitin chains that recruit the adaptor NEMO (NF-κB essential modulator; also known as IκB kinase γ [IKKγ]) and kinases TBK1 and IKKi (also known as IKK epsilon) (3–6). TBK1 and IKKi directly phosphorylate IRF3 and IRF7 to trigger their dimerization, nuclear localization, and activation of type I IFN to restrict virus replication (7, 8).

In addition to the production of type I IFN and proinflammatory cytokines, virus-induced apoptosis represents an important host mechanism for the inhibition of viral replication. IRF3 has been reported to localize to the mitochondria upon virus infection and interact with the proapoptotic protein Bax to trigger activation of the mitochondrial apoptotic pathway (9). Overexpression of MAVS induces apoptosis, which is countered by viral proteins including hepatitis C virus NS3/4A (10) and severe acute respiratory syndrome coronavirus (SARS-CoV) nonstructural protein NSP15 (11). How MAVS promotes caspase activation and apoptosis is poorly understood but likely involves direct interactions with proapoptotic effector proteins. MAVS inducibly interacts with mitogen-activated protein kinase (MAPK) kinase 7 (MKK7) in response to virus infection, which in turn activates c-Jun N-terminal kinase 2 (JNK2) to trigger apoptosis (12). MAVS interacts with the apoptosis adaptor proteins TRADD (13) and FADD (14) and can directly interface with caspase-8 during RNA virus infection to promote Bax/Bak-independent apoptosis (15). MAVS also modulates the stability of voltage-dependent anion channel 1 (VDAC1) to contribute to virus-induced apoptosis (16). However, host factors that regulate MAVS-mediated apoptosis have yet to be described.

TAX1BP1 was originally identified as an interacting protein of the human T-cell leukemia virus 1 (HTLV-1) Tax protein (17) and the NF-κB regulatory proteins A20 and TRAF6 by yeast two-hybrid screening (18, 19). TAX1BP1 serves as an adaptor molecule for the NF-κB inhibitor A20 to terminate NF-κB signaling and proinflammatory cytokine production (20, 21). TAX1BP1 recruits the E3 ligases Itch and RNF11 to A20 to form an inducible ubiquitin-editing complex that restricts proinflammatory signaling pathways (20, 22–24). TAX1BP1 also cooperates with A20 to restrict RIG-I/MDA5-mediated signaling and the induction of IFN-β during RNA virus infection by inhibiting the K63-linked polyubiquitination of TBK1 and IKKi (25). Recent studies indicate that TAX1BP1 also functions as a ubiquitin binding autophagy receptor that plays critical roles in autophagy-dependent clearance of *Salmonella enterica* serovar Typhimurium (26). TAX1BP1 may also function as an antiapoptotic protein (18) although little is known regarding its putative antiapoptotic activity.

In this report, we provide evidence that TAX1BP1 specifically inhibits virus-induced apoptosis but not cell death initiated by protein synthesis inhibitors or DNA damaging agents. TAX1BP1 translocates to mitochondria in response to RNA virus infection and inducibly interacts with the MAVS adaptor protein. TAX1BP1 recruits the E3 ligase Itch to MAVS to promote its ubiquitination and degradation. These findings provide new insight into the regulation of virus-induced cell death and also highlight a novel antiapoptotic function of TAX1BP1.

RESULTS

Loss of TAX1BP1 sensitizes cells to virus-induced apoptosis. In a previous study, we demonstrated that TAX1BP1 inhibits virus-triggered type I IFN by antagonizing K63-linked polyubiquitination of TBK1 and IKKi (25). Consistent with these findings, virus-induced expression of IFN-β mRNA was strongly upregulated in *Tax1bp1*$^{-/-}$ murine embryonic fibroblasts (MEFs) (Fig. 1A). As interferon produced in this manner would be expected to reduce virus replication and associated cytopathic effects (CPE), we were surprised to observe that *Tax1bp1*$^{-/-}$ MEFs instead manifested significantly increased CPE compared to levels in wild-type (WT) MEFs. As virus-induced CPE in *Tax1bp1*$^{-/-}$ MEFs bore the morphological features of apoptosis, we hypothesized that TAX1BP1, in parallel to its capacity to control IFN production, also regulated virus-induced apoptosis. To explore a potential role for TAX1BP1 in the regulation of virus-induced apoptosis, *Tax1bp1*$^{+/-}$ and *Tax1bp1*$^{-/-}$ MEFs were infected with the RNA virus vesicular stomatitis virus (VSV) at a multiplicity of infection (MOI) of 1. *Tax1bp1*$^{-/-}$ MEFs infected with VSV exhibited strong CPE, including shrinkage and rounding of cells, characteristic of apoptosis, as assessed by bright-field microscopy (Fig. 1B), while control *Tax1bp1*$^{+/-}$ MEFs were largely unaffected. To confirm that these results were not unique to mouse fibroblasts, the experiment was also conducted with

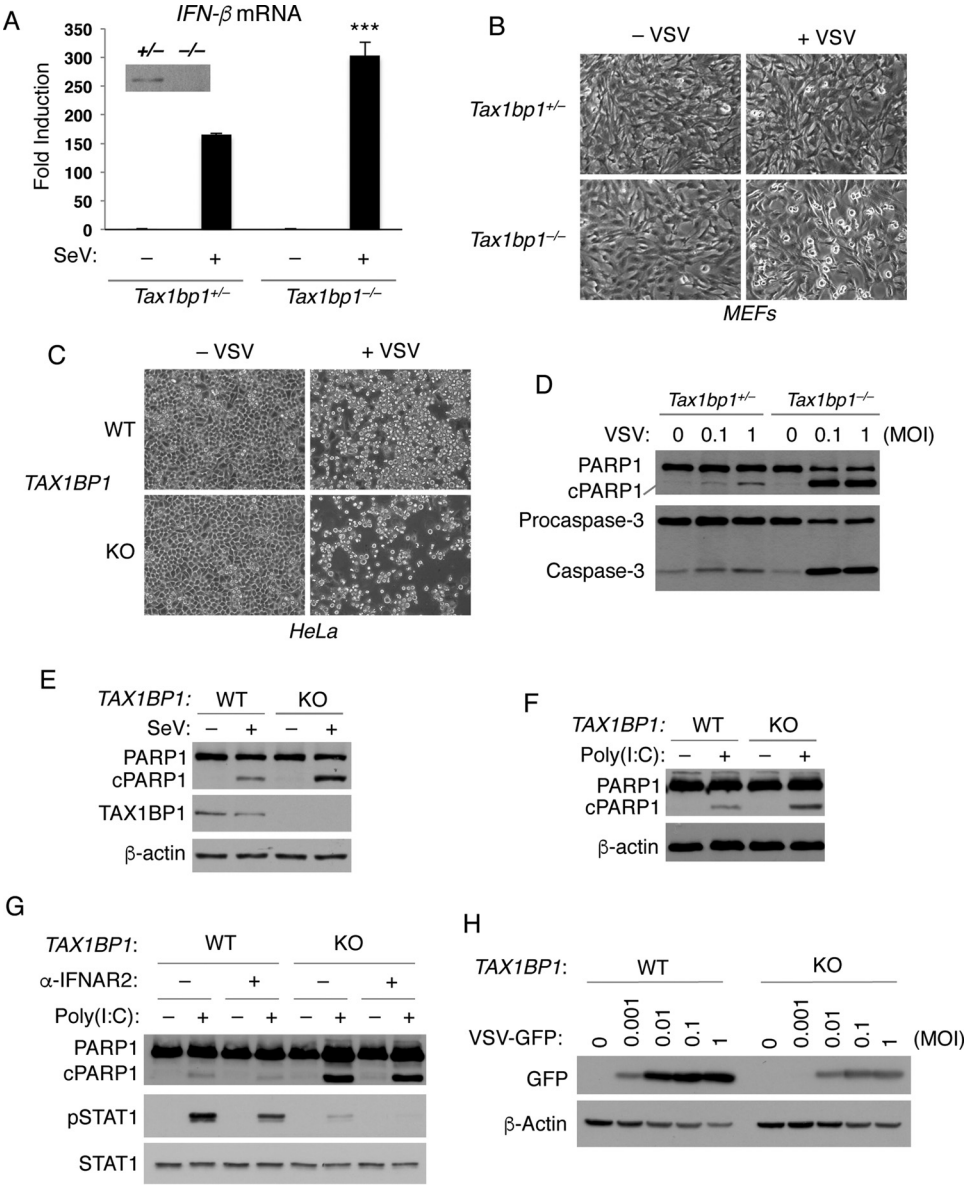

FIG 1 Loss of TAX1BP1 sensitizes cells to virus-induced cell death. (A) *Tax1bp1*$^{+/-}$ and *Tax1bp1*$^{-/-}$ MEFs were infected with SeV for 6 h. Total mRNA was extracted and subjected to qRT-PCR analysis for IFN-β expression. Western blotting confirms the absence of TAX1BP1 in *Tax1bp1*$^{-/-}$ MEFs. The values in the graph denote the means ± standard deviations. ***, $P < 0.0005$, for SeV-infected *Tax1bp1*$^{-/-}$ versus *Tax1bp1*$^{+/-}$ MEFs as determined by an unpaired Student's *t* test. (B and C) Phase-contrast images of TAX1BP1-deficient MEFs and HeLa cells infected with VSV. Images were taken at 6 h postinfection (MOI of 1) at magnifications of ×20 (B) and ×10 (C). (D) *Tax1bp1*$^{+/-}$ and *Tax1bp1*$^{-/-}$ MEFs were infected with VSV at the indicated MOIs. Total cell lysates were subjected to Western blotting with anti-PARP1 and caspase-3 antibodies. cPARP1 represents a cleavage product (87 kDa) of PARP1. (E and F) *TAX1BP1* WT and KO HeLa cells were infected with SeV (30 HA units/ml) for 24 h (E) or transfected with poly(I·C) (5 μg/ml) for 5 h (F). Total cell lysates were subjected to Western blotting with the indicated antibodies. (G) *TAX1BP1* WT and KO HeLa cells were pretreated with neutralizing anti-IFNAR2 antibody (5 μg/ml) for 30 min at 37°C and then transfected with 5 μg/ml poly(I·C) for 4 h. Cell extracts were subjected to Western blotting with the indicated antibodies. pSTAT1, phospho-STAT1. (H) *TAX1BP1* WT and KO HeLa cells were infected with VSV-GFP at the indicated MOIs for 20 h, and cell lysates were subjected to Western blotting with the indicated antibodies.

TAX1BP1 knockout (KO) HeLa cells, which have mutations in exon 3 of the *TAX1BP1* gene introduced by CRISPR/Cas9 technology (27). Consistently, increased susceptibility to the CPE of VSV was also observed in *TAX1BP1* KO HeLa cells (Fig. 1C).

To determine whether *Tax1bp1*$^{-/-}$ MEFs were undergoing apoptosis, lysates from *Tax1bp1*$^{+/-}$ and *Tax1bp1*$^{-/-}$ MEFs infected by VSV were subjected to Western blotting

for poly(ADP-ribose) polymerase 1 (PARP1) cleavage, a hallmark of apoptosis mediated by the executioner caspases 3 and 7 (28). Indeed, PARP1 cleavage was induced by VSV infection at multiple MOIs to a much greater degree in *Tax1bp1*$^{-/-}$ MEFs than in control MEFs (Fig. 1D). Consistently, virus-induced caspase-3 cleavage/activation was more robust in *Tax1bp1*$^{-/-}$ MEFs (Fig. 1D). *TAX1BP1* KO HeLa cells were also more sensitive to apoptosis after infection with Sendai virus (SeV) and transfection with the synthetic viral RNA analog poly(I·C) (Fig. 1E and F). Together, these results suggest that TAX1BP1 plays an important role in the protection of cells from virus-induced apoptosis.

Type I IFNs are known to sensitize cells to virus-induced apoptosis (29). To determine if the enhanced cell death in TAX1BP1-deficient cells was mediated by type I IFN signaling, *TAX1BP1* KO HeLa cells were pretreated with a neutralizing antibody to IFN-α/β receptor 2 (IFNAR2) prior to transfection with poly(I·C). Although the neutralizing antibody diminished poly(I·C)-induced STAT1 activation, there was no effect on PARP cleavage in *TAX1BP1* KO HeLa cells (Fig. 1G). Surprisingly, STAT1 phosphorylation was impaired in the absence of TAX1BP1 (Fig. 1G). Therefore, the enhanced virus or poly(I·C)-induced apoptosis in TAX1BP1-deficient cells is likely not attributable to type I IFN autocrine effects.

We next examined the replication of VSV encoding green fluorescent protein (VSV-GFP) (30) in control HeLa and *TAX1BP1* KO HeLa cells. Cells were infected with VSV-GFP at multiple MOIs (0, 0.001, 0.01, 0.1, and 1), and Western blotting was conducted to examine GFP expression as a readout of virus replication. Despite potential defects in type I IFN signaling, *TAX1BP1* KO HeLa cells were markedly resistant to VSV-GFP replication compared to control HeLa cells (Fig. 1H). These results indicate that the enhanced virus-induced apoptosis in TAX1BP1-deficient cells is likely the dominant mechanism that restricts virus replication.

TAX1BP1 overexpression was previously shown to inhibit apoptosis induced by TNF stimulation combined with the protein translation inhibitor cycloheximide (CHX) (18). Therefore, the antiapoptotic function of TAX1BP1 may extend beyond virus infection to a wider range of apoptotic stimuli. To examine this notion, *Tax1bp1*$^{-/-}$ and *Tax1bp1*$^{+/-}$ MEFs and *TAX1BP1* KO and control HeLa cells were treated with TNF plus CHX, staurosporine (STS), or etoposide, and apoptosis was quantified by flow cytometry after fluorescein isothiocyanate (FITC)-annexin V and 7-amino-actinomycin D (7-AAD) staining. STS is a protein kinase inhibitor that can trigger apoptosis. Etoposide is a topoisomerase inhibitor and DNA-damaging agent. As expected, SeV-induced apoptosis was significantly increased in both *Tax1bp1*$^{-/-}$ MEFs and *TAX1BP1* KO HeLa cells (Fig. 2A and B). However, STS-induced apoptosis was similar or diminished in TAX1BP1-deficient cells (Fig. 2A and B). Etoposide-mediated apoptosis was also slightly decreased in *TAX1BP1* KO HeLa cells (Fig. 2B). Although there was no difference in apoptosis in HeLa control and *TAX1BP1* KO HeLa cells treated with TNF plus CHX, there was a substantial increase in apoptosis in *Tax1bp1*$^{-/-}$ MEFs compared to the level in *Tax1bp1*$^{+/-}$ MEFs (Fig. 2A and B). These results may indicate cell-type-specific differences in the antiapoptotic function of TAX1BP1 in the TNF receptor (TNFR) pathway. Alternatively, the antiapoptotic function of TAX1BP1 downstream of death receptor signaling may be compromised in tumor cells. Nevertheless, our results are consistent with an earlier study showing that TAX1BP1 inhibits apoptosis induced by TNF plus CHX in NIH 3T3 cells but not in the A549 lung adenocarcinoma cell line (18). PARP1 cleavage levels in response to staurosporine and etoposide were also comparable in WT and *TAX1BP1* KO HeLa cells (Fig. 2C). Together, these results indicate that the antiapoptotic activity of TAX1BP1 is largely specific to virus infection although TAX1BP1 may also inhibit TNF-mediated apoptosis in specific cell types.

TAX1BP1 is degraded by virus infection. Based on published gene expression data (Affymetrix U133 Plus 2.0 arrays) retrieved from the Genevestigator's curated database (31, 32), TAX1BP1 expression is highest in the human cancer cell lines Hs 852.T (melanoma), LOU-NH91 (squamous cell lung carcinoma), and DLD1 (colon adenocar-

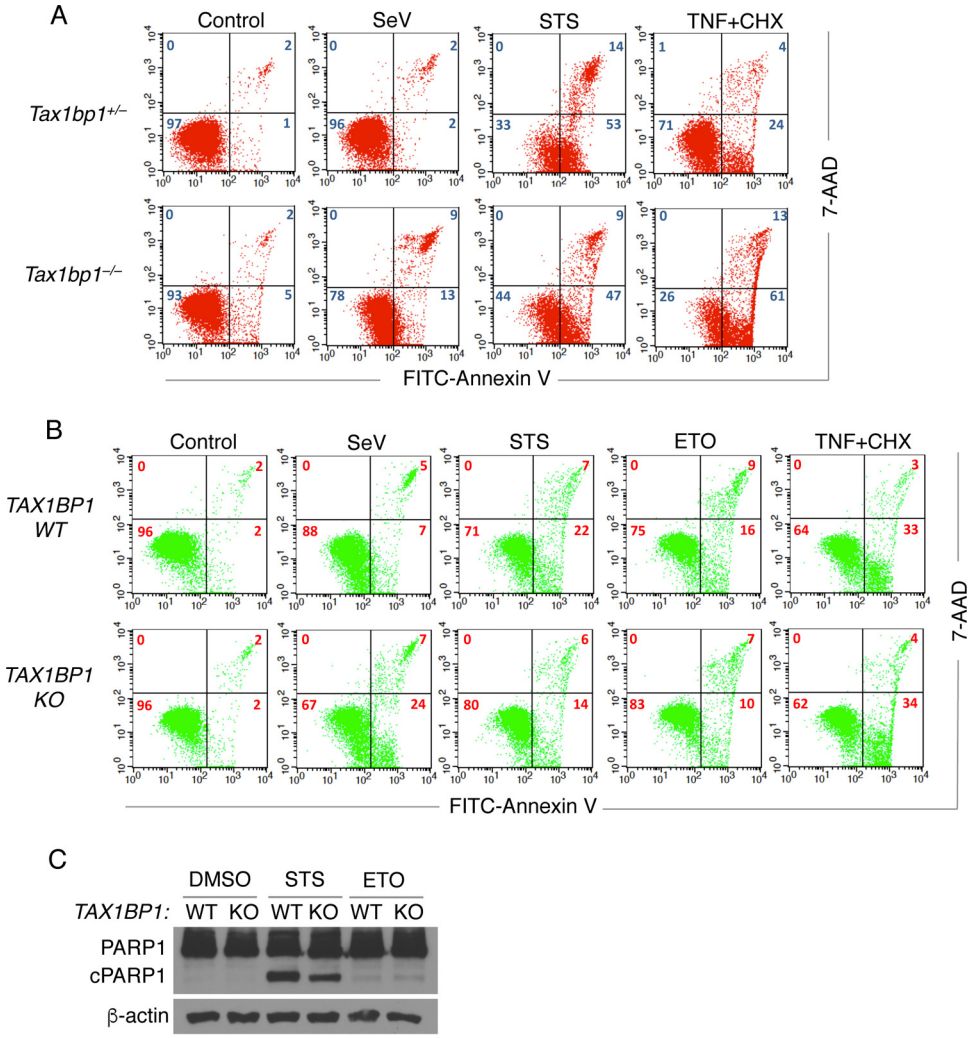

FIG 2 TAX1BP1 deficiency is largely selective for virus-induced apoptosis. (A and B) *Tax1bp1*$^{+/-}$ and *Tax1bp1*$^{-/-}$ MEFs (A) and *TAX1BP1* WT and KO HeLa cells (B) were infected with 30 HA units/ml SeV for 6 h or treated with 5 μM staurosporine (STS) for 4 h, 10 μM etoposide (ETO) for 24 h, or 20 ng/ml TNF-α plus 10 ng/ml cycloheximide (CHX) for 4 h. Cells were subjected to flow cytometric analysis upon staining with FITC-annexin V and 7-amino-actinomycin D (7-AAD). The percentages of cells in each quadrant are marked. (C) *TAX1BP1* WT and KO HeLa cells were treated with 5 μM staurosporine (STS) for 5 h or 10 μM etoposide (ETO) for 24 h. Total cell lysates were subjected to Western blotting with the indicated antibodies. DMSO, dimethyl sulfoxide.

cinoma), among 1,405 cell lines examined. Thus, we hypothesized that these tumor cell lines may exhibit resistance to virus-induced apoptosis owing to the elevated expression levels of TAX1BP1. However, transfection of poly(I·C) induced the cleavage of PARP1 in DLD1 cells after 4 h, indicating sensitivity to apoptosis (Fig. 3A). Surprisingly, TAX1BP1 protein was sharply diminished after 4 h of poly(I·C) transfection, coincident with PARP1 cleavage (Fig. 3A), thus raising the intriguing possibility that poly(I·C)-induced apoptosis in DLD1 cells is functionally linked to degradation of TAX1BP1. Similarly, TAX1BP1 was lost after infection with recombinant VSV-GFP for 24 h, coincident with PARP1 cleavage and GFP expression, indicative of VSV replication (Fig. 3B). TAX1BP1 degradation was not limited to tumor cell lines as it was also observed in primary mouse bone marrow-derived macrophages (BMDMs) infected with VSV (Fig. 3C). To provide further evidence that the reduction of TAX1BP1 protein was correlated with the increased sensitivity to virus-induced apoptosis in DLD1 cells, we generated two TAX1BP1 stable knockdown DLD1 cell lines using short hairpin RNAs (shRNAs) targeted to different regions of the TAX1BP1 transcript. Indeed, knockdown of TAX1BP1 sensitized DLD1 cells to poly(I·C)-induced apoptosis as revealed by increased PARP1

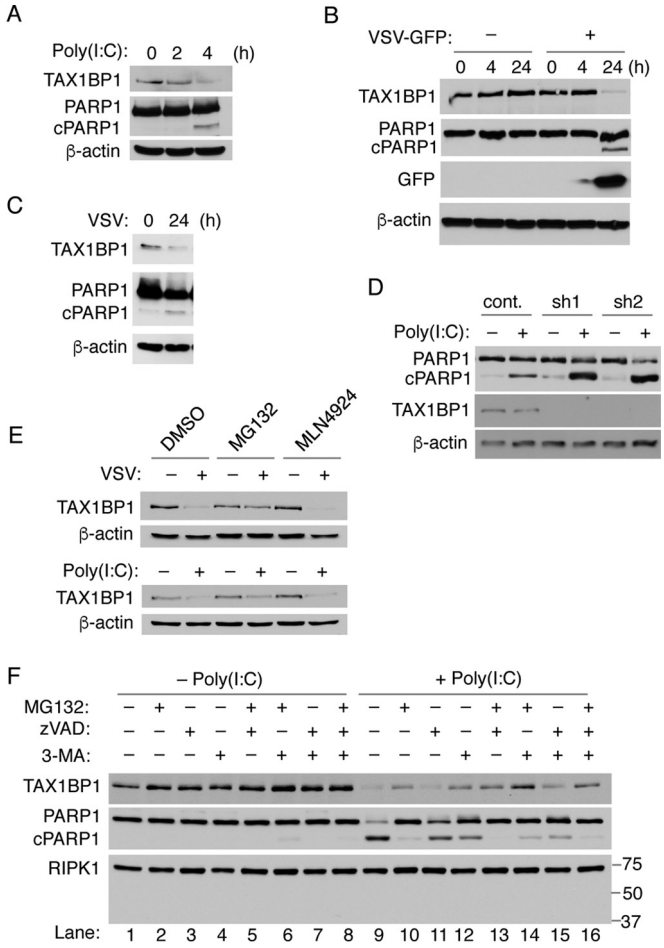

FIG 3 Virus-induced TAX1BP1 degradation increases susceptibility to apoptosis by virus infection. (A and B) DLD1 cells were transfected with poly(I·C) (5 μg/ml) or infected with recombinant VSV-GFP (MOI of 1) for the indicated times. Total cell lysates were subjected to Western blotting with the indicated antibodies. (C) Mouse BMDMs were infected with VSV (MOI of 1) for 24 h. Total cell lysates were subjected to Western blotting with the indicated antibodies. (D) DLD1 cells were stably transfected with control (cont.) short hairpin RNA (shRNA) and two TAX1BP1 shRNAs (sh1 and sh2) and transfected with poly(I·C) (5 μg/ml) for 4 h. Total cell lysates were subjected to Western blotting with the indicated antibodies. (E) DLD1 cells were pretreated with 10 μM MG132 and 5 μM MLN4924 for 1 h and then infected with VSV or transfected with poly(I·C) as described above. (F) DLD1 cells were pretreated with 10 μM MG132, 20 μM zVAD, or 10 mM 3-MA for 1 h and then transfected with poly(I·C). Total cell lysates were subjected to Western blotting with the indicated antibodies.

cleavage (Fig. 3D). Taken together, these results suggest that depletion or virus-induced degradation of TAX1BP1 evokes an apoptotic response.

We next sought to uncover the mechanism(s) of TAX1BP1 degradation elicited by virus infection. Recently, a quantitative proteomic analysis using stable isotope labeling with amino acids in cell culture (SILAC) revealed that TAX1BP1 is rapidly stabilized by treatment with MLN4924 (54), a selective inhibitor of the NEDD8-activating enzyme, suggesting that TAX1BP1 is a substrate of cullin-RING ubiquitin ligases (CRLs) for proteasomal degradation. However, TAX1BP1 degradation elicited by VSV infection or poly(I·C) transfection was not inhibited by MLN4924 (Fig. 3E). Instead, the proteasome inhibitor MG132 blocked TAX1BP1 degradation (Fig. 3E and F), suggesting that TAX1BP1 is subject to proteasomal degradation upon virus infection in a CRL-independent manner. We also examined a potential role of virus-activated caspases in TAX1BP1 degradation; however, the pan-caspase inhibitor zVAD (benzyloxycarbonyl-Val-Ala-Asp) did not inhibit poly(I·C)-induced TAX1BP1 degradation (Fig. 3F, lane 11).

Recent reports have suggested that TAX1BP1 may serve as a receptor for selective autophagy of bacteria (26) and mitochondria (33), raising the possibility that TAX1BP1

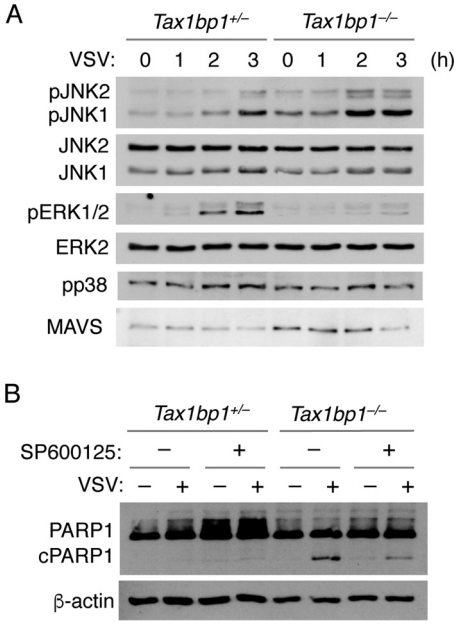

FIG 4 TAX1BP1 deficiency potentiates the activation of virus-induced proapoptotic signaling. (A) *Tax1bp1*$^{+/-}$ and *Tax1bp1*$^{-/-}$ MEFs were infected with VSV (MOI of 1) for the indicated times, and cell lysates were subjected to Western blotting with the indicated antibodies. (B) *Tax1bp1*$^{+/-}$ and *Tax1bp1*$^{-/-}$ MEFs were pretreated with 25 μM SP600125 for 1 h prior to infection with VSV (MOI of 1) for 6 h. Total cell lysates were subjected to Western blotting with the indicated antibodies.

is subject to autophagic degradation upon virus infection. To test this idea, cells were pretreated with 3-methyladenine (3-MA), an agent that interferes with the formation of autophagosomes. Indeed, 3-MA blocked poly(I·C)-induced TAX1BP1 degradation as effectively as MG132 (Fig. 3F, compare lanes 10 and 12). Furthermore, the combination of both inhibitors cooperatively blocked TAX1BP1 degradation (Fig. 3F, lane 14), indicating that TAX1BP1 degradation is mediated by both proteasomal and autophagic degradation pathways. It is noteworthy that MG132 strongly inhibited poly(I·C)-induced PARP1 cleavage compared to inhibition by zVAD and 3-MA (Fig. 3F), implying that additional antiapoptotic proteins might be stabilized by inhibition of proteasomal degradation. In this regard, we examined receptor-interacting serine/threonine kinase 1 (RIPK1), which can be cleaved by treatment with high doses of poly(I·C) (34). However, we were unable to detect any RIPK1 cleavage upon poly(I·C) transfection (Fig. 3F), supporting the involvement of the RIG-I-like receptor (RLR)-MAVS pathway in poly(I·C) transfection-induced apoptosis.

TAX1BP1 inhibits MAVS-mediated apoptosis following virus infection. A recent genetic study identified a novel MAVS-dependent apoptotic signaling pathway that is activated by RNA virus infection. In this pathway, MAVS recruits the kinase MKK7 to mitochondria, which in turn phosphorylate JNK2 to trigger apoptosis (12). As TAX1BP1 was previously found to regulate RNA virus-induced activation of type I IFN (25), we asked if TAX1BP1 might suppress the activation of MAVS-MKK7-JNK2-mediated cell death. To this end, we first examined virus-induced activation of MAPK signaling in *Tax1bp1*$^{+/-}$ and *Tax1bp1*$^{-/-}$ MEFs. As expected, all MAPKs examined, including JNK1/2, extracellular signal-regulated kinase 1 and 2 (ERK1/2), and p38, were phosphorylated upon VSV infection in *Tax1bp1*$^{+/-}$ MEFs (Fig. 4A). However, JNK1/2 phosphorylation was more robust in these cells, whereas the phosphorylation of p38 was slightly decreased, and phosphorylation of ERK1/2 was completely abrogated in *Tax1bp1*$^{-/-}$ MEFs compared to that in controls (Fig. 4A). These results suggest that TAX1BP1 may differentially regulate the activation of the MAPK pathways to promote cell survival in response to virus infection, for example, by activating ERK-mediated antiapoptotic signaling and by inhibiting JNK-mediated proapoptotic

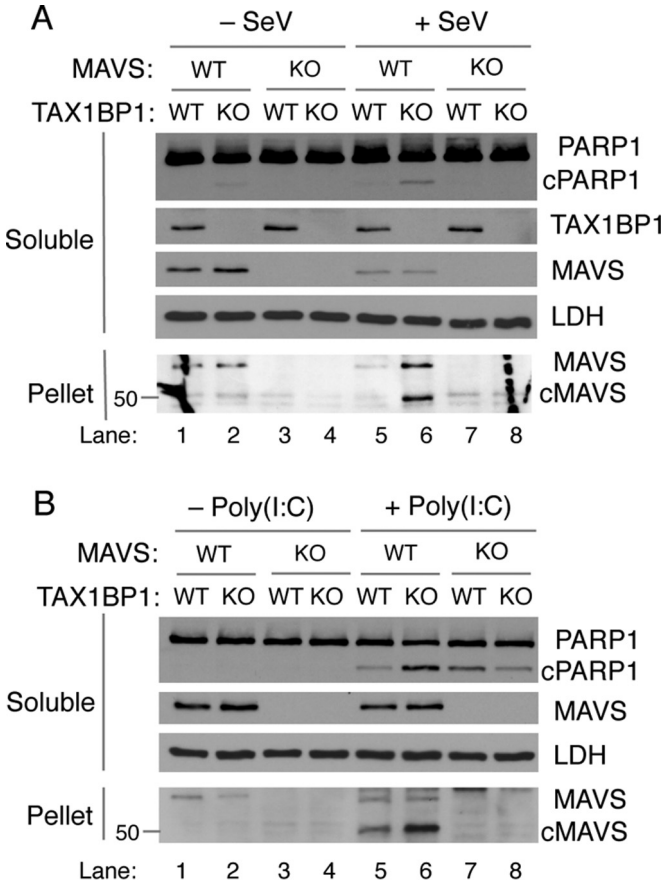

FIG 5 Virus-induced apoptosis in TAX1BP1-deficient cells is mediated by MAVS. HeLa cells deficient in TAX1BP1 and/or MAVS were infected with SeV (25 HA units/ml) for 24 h (A) or transfected with poly(I·C) (5 μg/ml) for 6 h (B). RIPA buffer-soluble (soluble) and insoluble (pellet) fractions were subjected to Western blotting with the indicated antibodies. Lactate dehydrogenase (LDH) was used as a loading control. cMAVS, a cleavage product of MAVS.

signaling. We next examined whether pharmacological inhibition of JNK could suppress virus-induced apoptosis in *Tax1bp1*$^{-/-}$ MEFs. Indeed, SP600125, a selective inhibitor of JNKs, partially blocked PARP1 cleavage induced by VSV infection in *Tax1bp1*$^{-/-}$ MEFs (Fig. 4B).

Overexpression of MAVS is sufficient for the expression of type I IFNs and the activation of apoptotic JNKs (11, 35), suggesting that the expression levels of MAVS protein may serve as a critical determinant for sufficient antiviral responses. Thus, we compared the levels of MAVS protein in total cell lysates derived from *Tax1bp1*$^{+/-}$ and *Tax1bp1*$^{-/-}$ MEFs. Interestingly, the basal level of MAVS protein was upregulated in *Tax1bp1*$^{-/-}$ MEFs relative to the level in *Tax1bp1*$^{+/-}$ MEFs (Fig. 4A). These results suggest that the enhanced sensitivity to virus-induced apoptosis in *Tax1bp1*$^{-/-}$ MEFs may be due in part to increased expression of MAVS protein. To test this idea, we generated double-KO HeLa cells lacking both TAX1BP1 and MAVS by editing the *MAVS* gene in *TAX1BP1* KO HeLa cells using CRISPR/Cas9 as described previously (35). Indeed, MAVS deficiency suppressed PARP1 cleavage induced by SeV infection and poly(I·C) transfection in *TAX1BP1* KO HeLa cells (Fig. 5A and B, respectively), indicating that TAX1BP1 inhibits virus-induced apoptosis that is mediated by MAVS.

Consistent with the increased basal level of MAVS protein in *Tax1bp1*$^{-/-}$ MEFs (Fig. 4A), levels of MAVS were also increased in *TAX1BP1* KO HeLa cells compared to levels in control cells (Fig. 5A and B, compare lanes 1 and 2). Furthermore, SeV infection and poly(I·C) transfection increased the amount of MAVS in the radioimmunoprecipitation assay (RIPA) buffer-insoluble fractions (pellet) derived from *TAX1BP1* KO HeLa cells

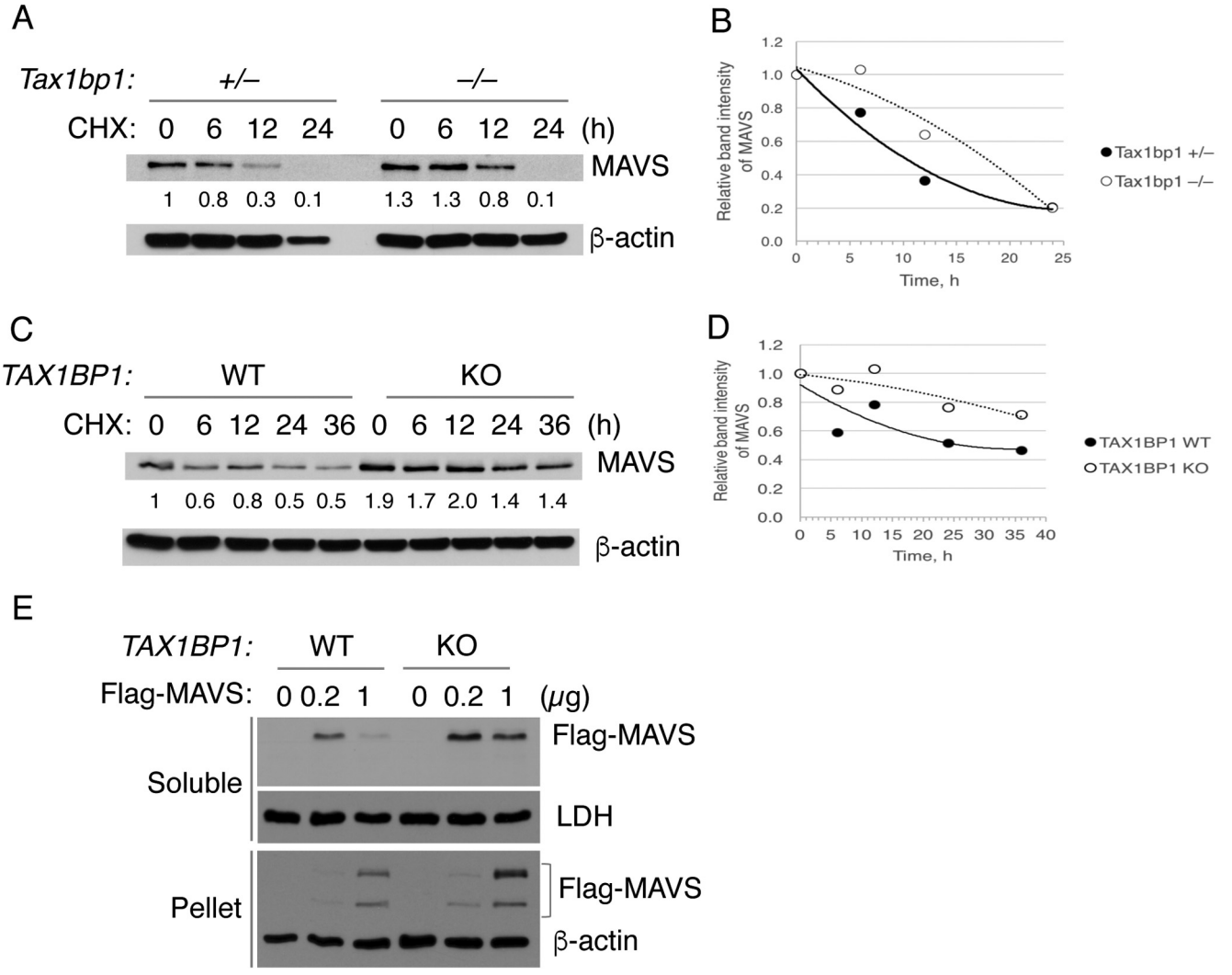

FIG 6 TAX1BP1 destabilizes MAVS protein. (A and C) Control and TAX1BP1-deficient MEFs (A) and HeLa cells (C) were treated with 10 μg/ml CHX for the indicated times, followed by Western blotting of the total cell lysates using anti-MAVS and -β-actin antibodies. Band intensity was measured using ImageJ software and normalized by the β-actin intensity. The relative MAVS levels compared to those of the CHX-untreated control cells are shown under the corresponding bands. (B and D) MAVS protein half-life in MEFs (B) and HeLa cells (D) was determined on graphs fitted by the second-order polynomial function. (E) *TAX1BP1* WT and KO HeLa cells were transiently transfected with 0.2 and 1 μg of Flag-MAVS plasmid. After 24 h, cells were fractionated into RIPA buffer-soluble (soluble) and insoluble (pellet) fractions, followed by Western blotting with the indicated antibodies.

(Fig. 5A and B, lanes 6). This result is consistent with a previous report indicating that MAVS translocates to the detergent-resistant membrane fractions following virus infection (3). Interestingly, the level of the faster-migrating MAVS protein (~50 kDa) was increased by SeV infection and poly(I·C) transfection (Fig. 5). Since the faster-migrating MAVS band was detected by a MAVS antibody raised against the N-terminal region encompassing amino acids 1 to 135, it does not likely represent miniMAVS, a smaller MAVS transcript with translation initiated at the second AUG codon (Met^{142}) (36). Instead, it likely represents a MAVS proteolysis product mediated by virus-activated caspases; for example, caspase-1 and caspase-3 cleave MAVS at residue D429 after dengue virus infection (37). Accordingly, an increase in the cleaved MAVS product may be indicative of apoptosis-associated caspase activation.

TAX1BP1 regulates MAVS stability. To further examine if TAX1BP1 regulates MAVS stability, we performed CHX chase assays. The basal level of MAVS protein in *Tax1bp1*$^{-/-}$ MEFs was higher (1.3-fold) than that in control MEFs (Fig. 6A), with a half-life extended by 8 h in *Tax1bp1*$^{-/-}$ MEFs (Fig. 6B). Similarly, the basal level of MAVS protein in *TAX1BP1* KO HeLa cells was higher (1.9-fold) than that in HeLa cells (Fig. 6C).

The half-life of MAVS was also extended in *TAX1BP1* KO HeLa cells compared to that in control cells (Fig. 6D). Next, we transfected HeLa cells with a Flag-MAVS plasmid at different concentrations to examine its stability in the absence or presence of TAX1BP1. As expected, Flag-MAVS was more readily detected in the RIPA-soluble fraction of *TAX1BP1* KO HeLa cells than in WT HeLa cells, consistent with the idea that MAVS is more stable in the absence of TAX1BP1 (Fig. 6E). We noticed that there was less MAVS protein detected in the soluble fraction when cells were transfected with Flag-MAVS at a higher concentration (1 μg) (Fig. 6E). Given that MAVS translocates to the RIPA buffer-insoluble fractions in response to virus infection, we reasoned that when Flag-MAVS is overexpressed, it may translocate to the detergent-insoluble fractions. Indeed, Flag-MAVS (transfected at 1 μg) was mostly found in the RIPA-insoluble fractions compared to its level in the soluble fractions in HeLa cells, with increased levels of full-length (FL) and cleaved MAVS (~50 kDa) in *TAX1BP1* KO HeLa cells (Fig. 6E). Taken together, these results suggest that TAX1BP1 modulates the outcome of apoptosis upon RNA virus infection by controlling the stability of MAVS.

TAX1BP1 interacts with MAVS and induces its polyubiquitination. MAVS has been shown to be downregulated by the ubiquitin-proteasome pathway in response to virus infection (38). To determine if TAX1BP1 could mediate virus-induced polyubiquitination of MAVS, we conducted ubiquitination assays in Flag-MAVS transfected WT and *TAX1BP1* KO HeLa cells. After SeV infection, Flag-MAVS was immunoprecipitated and then subjected to Western blotting with antiubiquitin and K48-linkage-specific ubiquitin antibodies. Indeed, virus-induced polyubiquitination (total ubiquitin) of MAVS was strongly induced in *TAX1BP1* WT HeLa cells but was not evident in *TAX1BP1* KO HeLa cells (Fig. 7A). Consistently, virus-induced K48-linked polyubiquitination of MAVS was absent in *TAX1BP1* KO HeLa cells (Fig. 7A), indicating that TAX1BP1 plays an essential role in virus-induced ubiquitination of MAVS.

To better understand the molecular basis for TAX1BP1 regulation of MAVS, we examined whether TAX1BP1 interacts with MAVS using a coimmunoprecipitation (co-IP) assay. In the same experiment, we also examined binding of TAX1BP1 with the HECT domain E3 ligase Itch, also termed atrophin-interacting protein 4 (AIP4) (23). *Tax1bp1*$^{+/+}$ and *Tax1bp1*$^{-/-}$ MEFs were infected with SeV for various times, and total cell lysates were subjected to IP using anti-TAX1BP1, followed by Western blotting with anti-MAVS and anti-Itch. Indeed, both MAVS and Itch were detected in the TAX1BP1 immunoprecipitates (in *Tax1bp1*$^{+/+}$ but not in *Tax1bp1*$^{-/-}$ MEFs) in an inducible manner after virus infection (Fig. 7B). SeV-induced IRF3 phosphorylation was detected in both *Tax1bp1*$^{+/+}$ and *Tax1bp1*$^{-/-}$ MEFs, indicating activation of RLR signaling (Fig. 7B).

Upon infection, MAVS is targeted to and polymerized on the mitochondrial outer membrane to induce type I IFN expression and apoptosis. Thus, we hypothesized that TAX1BP1 may translocate to mitochondria to interact with MAVS after virus infection. Indeed, subcellular fractionation experiments revealed that TAX1BP1 was localized at the mitochondria under basal conditions and was further increased by VSV infection (Fig. 7C). It is noteworthy that VSV infection induced the proteolysis of TAX1BP1 in the mitochondrial fraction (Fig. 7C). Consistent with the previous results, VSV infection resulted in the colocalization of TAX1BP1 with mitochondria (MitoTracker) in DLD1 cells (Fig. 7D).

To identify the region(s) of MAVS for TAX1BP1 binding, we transiently transfected 293T cells with full-length (FL) Flag-MAVS and deletion mutants lacking the caspase activation and recruitment domain (CARD), proline-rich domain (PD), and transmembrane (TM) domain, together with hemagglutinin (HA)-TAX1BP1. Total cell lysates and the Flag-immunoprecipitated proteins were probed with anti-HA and -Flag antibodies. HA-TAX1BP1 was coimmunoprecipitated with Flag-MAVS FL, ΔPD, and ΔTM but not ΔCARD (Fig. 7E), indicating that the CARD region of MAVS is essential for TAX1BP1 binding. To determine whether the interaction is required for TAX1BP1-mediated MAVS polyubiquitination, we performed ubiquitination assays using Flag-MAVS FL and

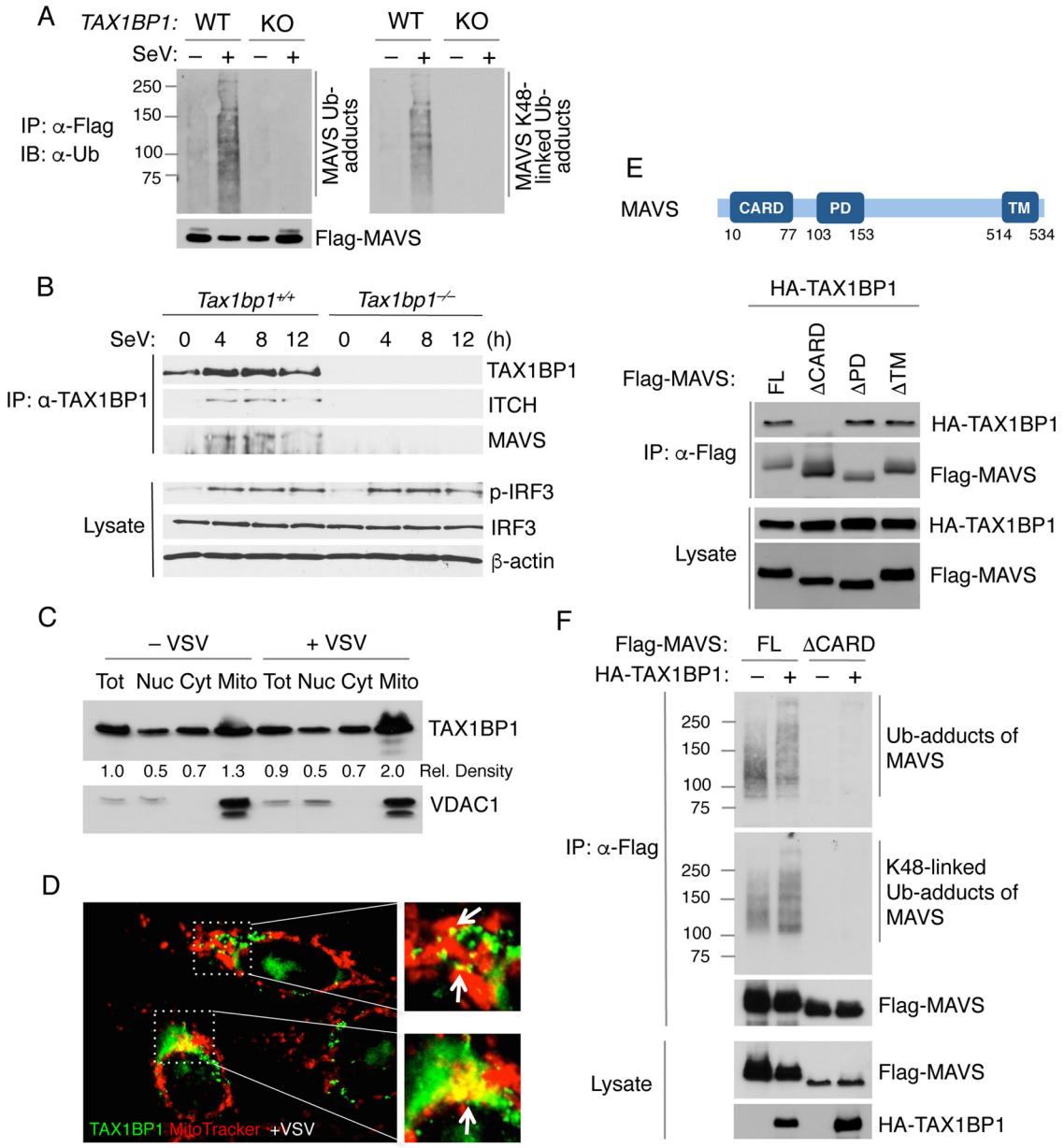

FIG 7 TAX1BP1 interacts with MAVS and induces its polyubiquitination. (A) *TAX1BP1* WT and KO HeLa cells were transfected with Flag-MAVS, treated with 10 μM MG132 for 1 h, and infected with SeV for 6 h. Total cell lysates were subjected to IP with anti-DYKDDDDK tag affinity gel followed by Western blotting with antiubiquitin (α-Ub), anti-K48-ubiquitin, and anti-Flag. (B) *Tax1bp1*$^{+/+}$ and *Tax1bp1*$^{-/-}$ MEFs were infected with SeV (25 HA units/ml) for the indicated times, and total cell lysates were subjected to co-IP assays with the indicated antibodies. (C) DLD1 cells were infected with VSV (MOI of 1) for 4 h and fractionated into nuclei (Nuc), cytosol (Cyt) and mitochondria (Mito). Homogenate was used as the total cell extract (Tot). A 40-fold excess of mitochondrial extracts versus total cell extract was loaded onto gels to achieve near normalization. Band intensity was measured using ImageJ software, and TAX1BP1 levels relative to those of the total cell extract of uninfected cells are shown under the corresponding bands. (D) DLD1 cells were infected with VSV as described above and incubated with 100 nM Red MitoTracker for 30 min prior to fixation for immunostaining with anti-TAX1BP1 antibody. The arrows indicate TAX1BP1 localized in mitochondria. (E) Depiction showing MAVS CARD, PD, and TM domain. 293T cells were transfected with HA-TAX1BP1 together with full-length (FL) Flag-MAVS and deletion mutants lacking the caspase activation and recruitment domain (ΔCARD), proline-rich domain (ΔPD), and transmembrane (ΔTM) domain. Total cell lysates were used for Flag-MAVS IP using anti-DYKDDDDK tag (L5) affinity gel. The IP and total cell lysates were resolved by SDS-PAGE and subjected to Western blotting with the indicated antibodies. (F) 293T cells were transfected with HA-TAX1BP1 together with Flag-MAVS FL or ΔCARD for ubiquitination assays using anti-Flag IP. The IP and total cell lysates were resolved by SDS-PAGE and subjected to Western blotting with the indicated antibodies.

ΔCARD in 293T cells. Overexpression of MAVS alone induced its mono- and polyubiquitination, but coexpression together with TAX1BP1 further promoted the elongation of polyubiquitin chains on MAVS protein (Fig. 7F). However, the MAVS ΔCARD mutant was defective in ubiquitination, and TAX1BP1 had no effect on its ubiquitination

(Fig. 7F), suggesting that the CARD of MAVS is involved in MAVS ubiquitination, potentially serving as a source of lysine residues for ubiquitination or recruiting ubiquitin E3 ligases for its ubiquitination. Indeed, TRIM25 was reported to induce MAVS polyubiquitination on lysine 10, which is lacking in the MAVS ΔCARD mutant (39). However, it is unknown if MAVS recruits E3 ligases via its CARD.

TAX1BP1 mediates the interaction of MAVS and the E3 ligase Itch. Poly(C)-binding protein 1 (PCBP1) and PCBP2 have been implicated in the ubiquitination and degradation of MAVS via the E3 ligase Itch (40, 41). In particular, the MAVS C-terminal region (residues 360 to 540 and 460 to 510), but not the CARD, was necessary for PCBP1 and PCBP2 binding, respectively (41, 42). We previously found that TAX1BP1 could interact directly with Itch via its two PPXY (P, proline; X, any amino acid; Y, tyrosine) motifs embedded within the C-terminal UBZ domains (23). Thus, we surmised that TAX1BP1 could mediate the ubiquitination and degradation of MAVS by recruiting Itch through the CARD of MAVS. First, we examined the activation of virus-induced MAPK signaling pathways in *Itch*$^{-/-}$ MEFs. Analogous to the results in *Tax1bp1*$^{-/-}$ MEFs (Fig. 4A), VSV-induced JNK1/2 activation was augmented whereas ERK1/2 activation was diminished in *Itch*$^{-/-}$ MEFs compared to levels in *Itch*$^{+/+}$ MEFs (Fig. 8A). In addition, VSV-induced apoptosis (PARP1 cleavage) was increased, and the basal level of MAVS protein was elevated in *Itch*$^{-/-}$ MEFs (Fig. 8A). The increased MAVS protein expression in *Itch*$^{-/-}$ MEFs was likely due to its impaired ubiquitination and proteasomal degradation. Indeed, transfected MAVS underwent SeV-induced K48-linked polyubiquitination in *Itch*$^{+/+}$ MEFs but not in *Itch*$^{-/-}$ MEFs (Fig. 8B). These results suggest that Itch inhibits MAVS protein expression and antagonizes MAVS-mediated apoptosis following virus infection.

To determine if TAX1BP1 is required for mediating the interaction between MAVS and Itch, we performed co-IP assays using *Tax1bp1*$^{+/+}$ and *Tax1bp1*$^{-/-}$ MEFs. Cells were infected with SeV for various times, and total cell lysates were subjected to IP using anti-MAVS, followed by Western blotting with anti-Itch and anti-TAX1BP1. MAVS interacted with Itch in a virus-inducible manner in control MEFs; however, this interaction was lost in *Tax1bp1*$^{-/-}$ MEFs (Fig. 8C). MAVS weakly interacted with TAX1BP1 under basal conditions, but SeV infection strongly promoted their interactions (Fig. 8C). MAVS-associated TAX1BP1 also appeared to be heavily phosphorylated, as indicated by the slower-migrating TAX1BP1 bands on Western blots (Fig. 8C). SeV-induced IRF3 phosphorylation was detected in both *Tax1bp1*$^{+/+}$ and *Tax1bp1*$^{-/-}$ MEFs, thus confirming virus-induced RLR signaling in these cells (Fig. 8C). Together, these data support the idea that TAX1BP1 is necessary for the interaction of MAVS and Itch.

To address the functional importance of the interaction between TAX1BP1 and Itch in the regulation of MAVS stability, we generated single (Y741A or Y768A) and double (Y741A and Y768A) mutants of the two PPXY motifs in the context of TAX1BP1 isoform 1 (Fig. 8D) and transfected these together with Flag-MAVS. HA-TAX1BP1 and single PPXY mutants reduced the level of MAVS, but the double PPXY mutant (A741/A768) largely lost its ability to downregulate MAVS (Fig. 8D), indicating that the two PPXY motifs of TAX1BP1 are important for MAVS degradation. Next, we performed ubiquitination assays to determine if the PPXY motifs of TAX1BP1 were involved in MAVS polyubiquitination. 293T cells were transfected with Flag-MAVS together with WT HA-TAX1BP1 and the PPXY double mutant (Y741A Y768A). Indeed, WT TAX1BP1 strongly promoted MAVS polyubiquitination (both total and K48 linked) in insoluble fractions (Fig. 8E); however, MAVS ubiquitination was clearly reduced when the two PPXY motifs in TAX1BP1 were mutated (Fig. 8E). Furthermore, WT TAX1BP1, but not the PPXY double mutant, promoted an interaction between MAVS and Itch (Fig. 8F). Together, these findings support the idea that TAX1BP1 serves as an adaptor molecule for Itch to target MAVS for K48-linked polyubiquitination and degradation.

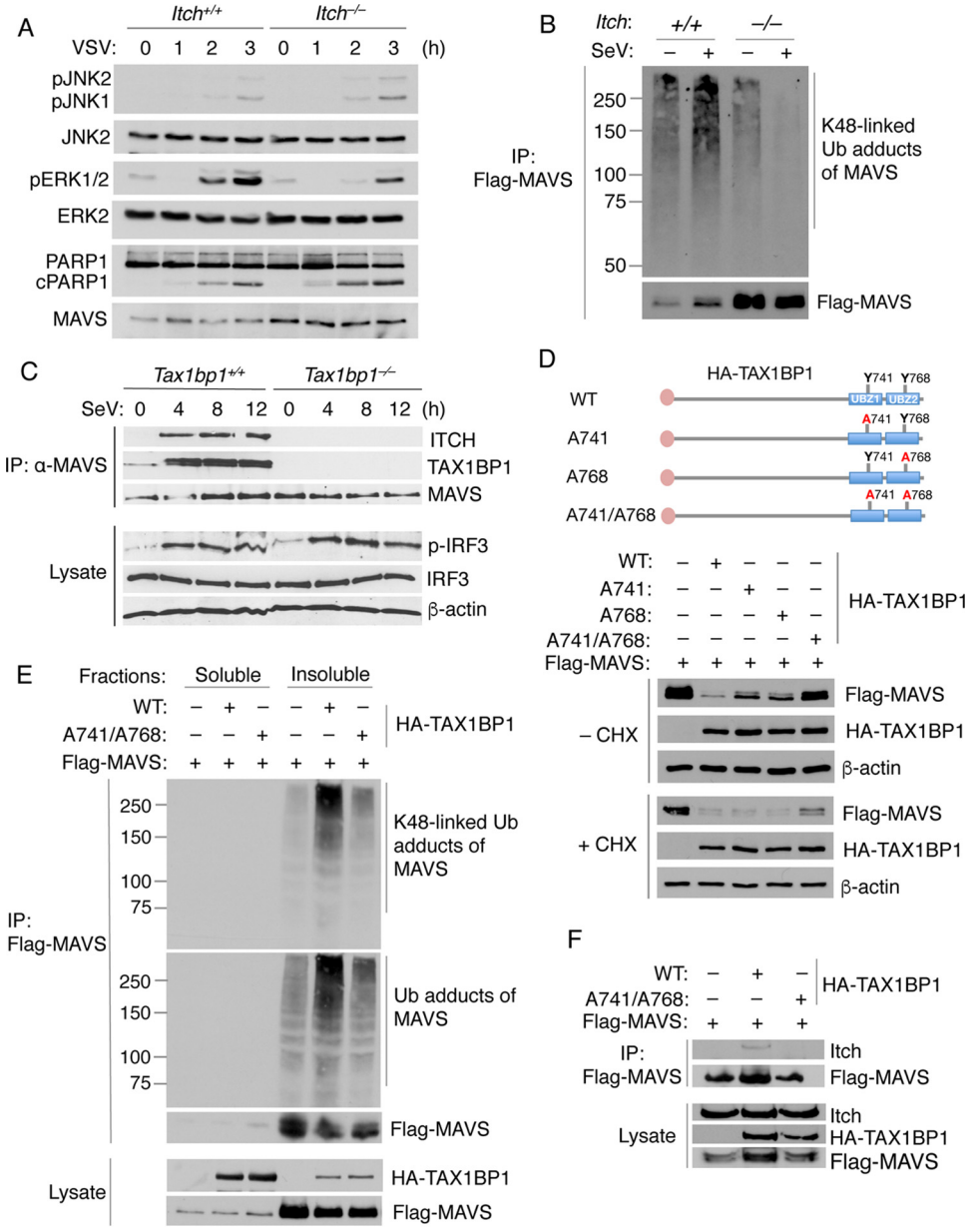

FIG 8 Itch cooperates with TAX1BP1 to promote MAVS degradation. (A) *Itch*$^{+/+}$ and *Itch*$^{-/-}$ MEFs were infected with VSV (MOI of 1) for the indicated times, and total cell lysates were subjected to Western blotting with the indicated antibodies. (B) *Itch*$^{+/+}$ and *Itch*$^{-/-}$ MEFs were transfected with a Flag-MAVS plasmid for 24 h, treated with 10 μM MG132 for 1 h, and infected with SeV (30 HA units/ml) for 6 h. Sonicated total cell extracts were used for ubiquitination assays, and immunoprecipitated proteins were subjected to Western blotting with antibodies specific for K48-linked ubiquitin (Ub) and Flag. (C) *Tax1bp1*$^{+/+}$ and *Tax1bp1*$^{-/-}$ MEFs were infected with SeV (25 HA units/ml) for the indicated times, and total cell lysates were subjected to co-IP assays with the indicated antibodies. (D) Single and double mutations (Y741A and Y768A) of the two PPXY motifs of TAX1BP1 were generated as shown in the diagram. 293T cells were transfected with plasmids expressing Flag-MAVS and HA-TAX1BP1 (WT or mutants) at a ratio of 1 to 9 for 24 h and then treated with (+) or without (−) 10 μg/ml CHX for an additional 6 h. Total cell lysates were subjected to Western blotting with the indicated antibodies. (E) 293T cells were transfected with the indicated plasmids, and after 24 h cells were fractionated into RIPA buffer-soluble and -insoluble fractions. Each fraction was used for ubiquitination assays and Western blotting. (F) TAX1BP1 KO HeLa cells were transfected with the indicated plasmids for 24 h, and sonicated total cell lysates were used for co-IP assays. The immunoprecipitated complex and cell lysates were subjected to Western blotting with the indicated antibodies.

DISCUSSION

In this study, we have provided several lines of evidence supporting TAX1BP1 as a potent negative regulator of MAVS-mediated antiviral apoptosis. First, TAX1BP1-deficient cells exhibited increased basal levels and a prolonged half-life of MAVS

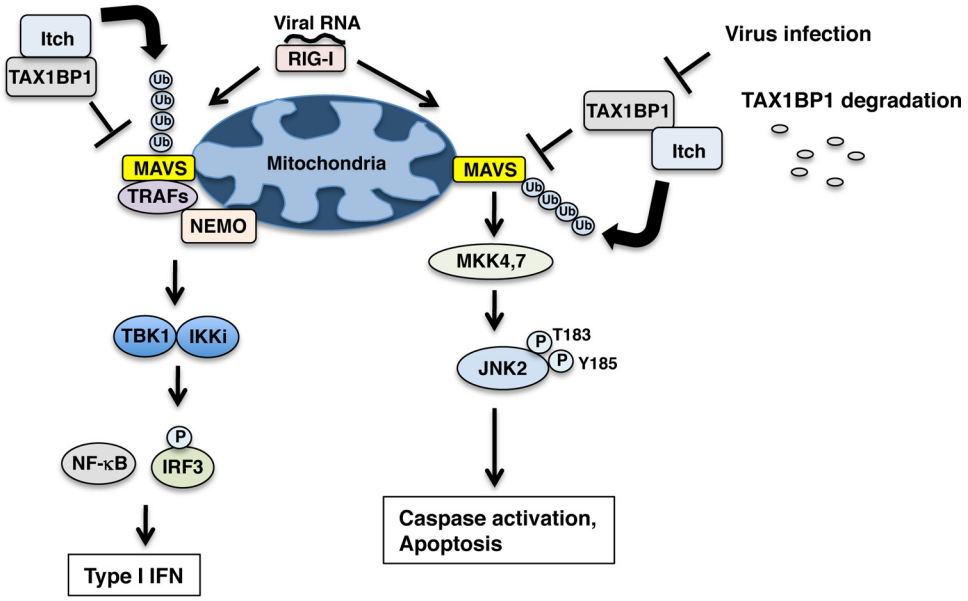

FIG 9 Schematic of the role of TAX1BP1 in RNA virus-induced apoptosis. TAX1BP1 interacts with MAVS and triggers its ubiquitination and degradation by recruiting the E3 ligase Itch. During virus infection, TAX1BP1 is degraded, and increased MAVS expression promotes type I IFN and JNK-induced apoptosis.

protein. Second, TAX1BP1 deficiency resulted in the accumulation of MAVS in the detergent-insoluble fractions upon its overexpression and virus infection. Third, TAX1BP1 interacted with the CARD of MAVS and recruited the ubiquitin E3 ligase Itch to induce MAVS polyubiquitination and degradation. Fourth, virus infection induced TAX1BP1 localization to mitochondria where it interacted with MAVS. Therefore, TAX1BP1 is a mitochondrion-targeting adaptor molecule that modulates virus-induced apoptosis by facilitating Itch-induced MAVS degradation (Fig. 9). TAX1BP1 regulation of MAVS likely represents a mechanism that enforces the tight regulation of MAVS protein levels to prevent exaggerated host antiviral signaling that may result in deleterious inflammatory effects on the host.

In addition to TAX1BP1, other adaptors have been reported to mediate MAVS degradation and inhibit MAVS-mediated antiviral innate immune responses. The inhibitory proteins PCBP1 and PCBP2 bind to the C-terminal region of MAVS and recruit Itch to induce the K48-linked polyubiquitination of MAVS for proteasome-mediated degradation (40, 41). PCBP1 mediates housekeeping or basal degradation of MAVS (41) while PCBP2 facilitates virus infection-induced MAVS degradation (40). Our data indicate, however, that TAX1BP1 could mediate both basal and virus-induced MAVS degradation utilizing the same ubiquitin E3 ligase, Itch, as PCBP1/2. This discrepancy could be explained by their different binding sites on MAVS. MAVS ubiquitination at lysines 371 and 420 by PCBP2/Itch promotes the degradation of MAVS (40). However, other lysine residues, including K7, K10, and K500, on MAVS can also be ubiquitinated by other ubiquitin E3 ligases for its degradation following virus infection (39, 43). Indeed, our data indicate that TAX1BP1 was unable to promote the ubiquitination of the MAVS ΔCARD mutant lacking K10 (Fig. 7F). Thus, it is plausible that TAX1BP1/Itch may regulate MAVS degradation independently or cooperatively with PCBP/Itch complexes although the ubiquitination residues for TAX1BP1/Itch-mediated MAVS degradation have yet to be identified. In addition to TAX1BP1 and PCBP1/2, another adaptor, Ndfip1, was also reported to induce MAVS degradation by recruiting the ubiquitin E3 ligase Smurf1 (44). The complexity of the MAVS degradation pathways is further highlighted by other ubiquitin E3 ligases, including MARCH5 (43), RNF5 (45), GP78 (46), Smurf2 (47), TRIM25 (39), and pVHL (48), that may interact with and target MAVS for degradation. Nevertheless, the effect of MAVS degradation on virus-induced apoptosis was not addressed in these previous studies. Therefore, to our knowledge our findings are the

first to describe proteasomal degradation of MAVS as a mechanism to suppress virus-induced apoptosis.

Our results have also revealed that TAX1BP1 undergoes degradation, both via the proteasome and autophagy (Fig. 3E and F), upon virus infection, and its degradation is tightly linked with cell death. Therefore, TAX1BP1 degradation likely constitutes a host mechanism to relieve MAVS-mediated inhibition and promote both IFN production and rapid apoptosis to limit virus spread. Future studies are needed to address the mechanisms by which virus infection induces TAX1BP1 degradation. In this regard, we previously found that overexpression of the kinases TBK1 and IKKi caused a slower migration of TAX1BP1 in Western blotting, indicative of TAX1BP1 phosphorylation (25). It also appears that MAVS-associated TAX1BP1 may be phosphorylated after SeV infection (Fig. 8C). It is tempting to speculate that TBK1/IKKi phosphorylation of TAX1BP1 triggers its degradation and resulting cell death. The identification of a TAX1BP1 phosphorylation site(s) and of the E3 ubiquitin ligase represents an important area for future research.

The antiapoptotic function of TAX1BP1 appears to be specific to virus infection but not in response to DNA-damaging agents or protein synthesis inhibitors (Fig. 1 and 2). TAX1BP1 may also regulate apoptosis downstream of death receptors such as TNFR (Fig. 2) although this function may be cell type specific or impaired in tumor cell lines such as HeLa. TAX1BP1 targeting of MAVS for ubiquitination and degradation likely represents the mechanism by which TAX1BP1 restricts virus-induced apoptosis. Interestingly, viral proteins such as HTLV-1 Tax and human papillomavirus (HPV) E2 have been shown to interact with TAX1BP1 (49). It is conceivable that viruses specifically target TAX1BP1 as a mechanism to inhibit cell death triggered by virus infection. It remains to be seen if these viral proteins exert any effect on virus-induced TAX1BP1 degradation.

In summary, our findings have revealed a novel molecular mechanism whereby TAX1BP1 inhibits virus-induced apoptosis by inducing the K48-linked polyubiquitination and degradation of MAVS via recruitment of Itch, thereby attenuating MAVS-mediated apoptosis signaling.

MATERIALS AND METHODS

Plasmids and oligonucleotides. The plasmid expressing Flag-human TAX1BP1 isoform 1 (amino acids 1 to 789) was described previously (50). To generate HA-TAX1BP1, the cDNA of TAX1BP1 was PCR amplified and inserted between the SalI and NotI sites of pRK5-HA. Plasmids expressing Flag-MAVS and deletion mutants lacking the CARD, PD, and TM regions were described previously (35). Site-directed mutagenesis and cDNA PCR amplification were conducted using Platinum Pfx DNA polymerase (Invitrogen). The short hairpin RNAs (shRNAs) of TAX1BP1 were inserted between the BamHI and MluI sites of lentiviral transfer vector pYNC352/puro as described previously (51): TAX1BP1 shRNA1, 5′-TTACACCTTA ACTCCATATAT-3′; TAX1BP1 shRNA2, 5′-GGAGTACTGCTCGTGATTATT-3′. For CRISPR/Cas9-mediated genome editing, a guide RNA (gRNA) specific to the *MAVS* gene was cloned into LentiCRISPR-V2 vector (a gift from Feng Zhang; Addgene plasmid 52961) using the BsmBI enzyme site as previously described (35). The MAVS gRNA sequence is 5′-CAGGGAACCGGGACACCCTC-3′. The sequences of primers used for quantitative real-time PCR are as follows: mouse IFN-β, 5′-TACGGTTGGCGAAGTCACATC-3′ (forward) and 5′-CCTCGCAGCAGACTACACCTCCAC-3′ (reverse); mouse glyceraldehyde-3-phosphate dehydrogenase (GAPDH), 5′-AGGTCGGTGTGAACGGATTTG-3′ (forward) and 5′-TGTAGACCATGTAGTTGAGGTCA-3′ (reverse).

Antibodies. Anti-MAVS (sc-166583), VDAC1 (sc-390996), lactate dehydrogenase (LDH; sc-33781), GFP (sc-8334), caspase-3 (sc-7148), JNK2 (sc-827), and ERK2 (sc-154) antibodies were purchased from Santa Cruz Biotechnology (Dallas, TX). Anti-PARP (catalog number 9532), phospho-JNK1/2 (Thr183/Tyr185) (4668), SAPK/JNK (9252), phospho-ERK1/2 (Thr202/Tyr204) (9101), phospho-p38 MAPK (4511), TAX1BP1 (5101), RIPK1 (3493), rodent-specific MAVS (4983), and K48-linkage specific polyubiquitin (4289) antibodies were purchased from Cell Signaling Technology (Danvers, MA). Antiubiquitin (ADI-SPA-200) antibody was purchased from ENZO Life Science (Farmingdale, NY). Anti-HA antibody (clone 12CA5) was purchased from Roche Applied Science (Indianapolis, IN). Rabbit polyclonal anti-MAVS (residues 150 to 200) antibody (lot A300-782A) was purchased from Bethyl Laboratories (Montgomery, TX). Anti-TAX1BP1 (ab22049 and ab176572) antibodies were purchased from Abcam (Cambridge, MA). Anti-Flag (M2) (F1804) and β-actin (A1978) antibodies were purchased from Sigma-Aldrich (St. Louis, MO). Anti-IFNAR2 antibody (clone MMHAR-2) was from PBL Assay Science (Piscataway, NJ). Anti-DYKDDDDK tag (L5) affinity gel was purchased from BioLegend (San Diego, CA).

Cell culture, transfection, and virus infection. Mouse embryonic fibroblasts (MEFs), HeLa, and 293T cells were cultured in Dulbecco's modified Eagle medium (DMEM) supplemented with 10% fetal bovine

serum and 20 units/ml penicillin-streptomycin. *Tax1bp1*$^{+/-}$ and *Tax1bp1*$^{-/-}$ MEFs were previously described (20). *TAX1BP1* knockout (KO) HeLa cells were provided by Richard Youle (27). Mouse bone marrow-derived macrophages (BMDMs) were obtained by culturing bone marrow cells (isolated from C57BL/6 femurs) with L929 conditioned medium for 7 days as described previously (52). C57BL/6 mice were housed under pathogen-free conditions at the Johns Hopkins University School of Medicine, in accordance with the Institutional Animal Care and Use Guidelines. Transient and stable transfections with plasmids were performed using GenJet version II (SignaGen Laboratories, Rockville, MD) according to the manufacturer's instruction. For virus infection, cells were serum starved for 1 h, inoculated with vesicular stomatitis virus (VSV) or Sendai virus (SeV) in serum-free DMEM for 1 h, and further incubated in complete DMEM. For generation of MAVS-deficient cells, *TAX1BP1* wild-type (WT) and KO HeLa cells were stably transfected with LentiCRISPR V2-MAVS gRNA in the presence of puromycin and subjected to cell cloning by limiting dilution.

Immunological analyses. Cells were lysed on ice for 1 h in RIPA buffer (50 mM Tris-HCl [pH 7.4], 150 mM NaCl, 1% Igepal CA-630, 0.25% deoxycholate, 10 mM NaF, and 10 mM Na_3VO_4) freshly supplemented with protease inhibitor cocktail (Roche Applied Bioscience, Indianapolis, IN) and centrifuged at 20,000 $\times$ *g* for 10 min. The pellet fraction was solubilized by boiling in 1$\times$ SDS sample buffer (62.5 mM Tris-HCl [pH 6.8], 2% SDS, 10% glycerol, 0.01% bromophenol blue, and 125 mM dithiothreitol) or by sonication (see below) in RIPA buffer and used as the detergent-insoluble fraction. For preparation of total cell lysates, cells were sonicated in RIPA buffer for 10 min at a high power setting (320W) using a Bioruptor (Diagenode, Denville, NJ). Sonicated samples were cleared of debris by centrifugation. For Western blotting, cell lysates were separated by SDS-PAGE, transferred to nitrocellulose membranes, and immunoblotted with appropriate antibodies diluted in SuperBlock blocking phosphate-buffered saline (PBS) buffer (Thermo Scientific, Rockford, IL). The immunoreactive bands were visualized by enhanced chemiluminescence (ECL) reagents (Perkin-Elmer). For immunoprecipitation (IP), cell lysates were incubated at 4°C overnight with antibody and incubated with protein A-agarose beads for an additional 3 h, and the immunoprecipitates were washed three times in RIPA buffer. For the immunoprecipitation of Flag-tagged proteins, anti-DYKDDDDK tag (L5) affinity gel was used. For ubiquitination assays, an extra wash was performed using RIPA buffer supplemented with 1 M urea after IP. For immunostaining, cells were fixed and permeabilized in chilled methanol for 10 min. For staining of mitochondria, cells were incubated with 100 nM Red MitoTracker (Invitrogen, Grand Island, NY) for 30 min before fixation. Following incubation with SuperBlock blocking PBS buffer overnight at 4°C, coverslips were incubated with primary antibodies, washed with PBS, and then incubated with appropriate fluorescent dye-conjugated secondary antibodies. Stained cells were imaged on a Nikon E800 microscope with a 60$\times$ oil-corrected objective and Element software.

Flow cytometric analysis of apoptosis. After stimulation with apoptosis inducers or infection with virus, floating and adherent MEFs or HeLa cells were harvested and washed with ice-cold PBS twice. Accutase (ThermoFisher Scientific) was used to detach adherent cells. Cells were resuspended in a solution of FITC-labeled annexin V and 7-amino-actinomycin D (7-AAD) in 100 μl of binding buffer (BioLegend). After incubation for 15 min at room temperature in the dark, cell suspensions were analyzed by flow cytometry using a FACSCalibur (BD Biosciences) flow cytometer.

Subcellular fractionation. Pure mitochondria were isolated using Axis-Shield OptiPrep iodixanol (Sigma-Aldrich, St. Louis, MO) as previously described (35). Briefly, cultured cells were homogenized in buffer B (0.25 M sucrose, 1 mM EDTA, 20 mM HEPES-NaOH [pH 7.4]) with 30 strokes of a Dounce glass homogenizer and centrifuged at 1,000 $\times$ *g* for 10 min. An aliquot of the homogenate was used as the total cell lysate. The homogenate was centrifuged at 1,000 $\times$ *g* for 10 min at 4°C, and the pellet was used as the nuclear fraction. The supernatant was further centrifuged at 13,000 $\times$ *g* for 10 min. The pellet was resuspended in 36% iodixanol, bottom loaded under 10% and 30% iodixanol gradients, and centrifuged at 50,000 $\times$ *g* for 4 h. The mitochondria were collected at the 10%/30% iodixanol interface.

Cycloheximide chase assay. Cells were treated with 10 μg/ml of cycloheximide (CHX). Total cell lysates were prepared in RIPA buffer using a sonicator, resolved by SDS-PAGE, and subjected to Western blotting with anti-MAVS. The intensity of MAVS bands was determined using ImageJ software (53) and normalized by β-actin bands on a parallel gel. The MAVS band intensity relative to that of CHX-untreated controls is indicated under the bands and depicted in the line graph.

qRT-PCR. Total RNA was isolated using an RNeasy minikit (Qiagen, Valencia, CA). First-strand cDNA was synthesized from 1 μg of total RNA using SuperScript V reverse transcriptase (Invitrogen) with random hexamers. Quantitative real-time PCR (qRT-PCR) was performed in a 96-well microplate using an ABI Prism 7500 detection system (Applied Biosystems, Foster City, CA) with KiCqStart SYBR green qPCR Readymix (Sigma). Reactions were performed in a total volume of 25 μl and contained 50 ng of reverse-transcribed RNA (based on the initial RNA concentration).

ACKNOWLEDGMENTS

We thank Richard Youle (NIH) and Lydia Matesic (University of South Carolina) for the *TAX1BP1* KO HeLa cells and *Itch*$^{-/-}$ MEFs, respectively.

This work was supported by National Institutes of Health grants RO1CA135362, R21AI112763 (to E.W.H.), and R21AI117168 (to Y.B.C.) and also in part by NCI Center Support Grant P30 CA006973.

REFERENCES

1. Hornung V, Ellegast J, Kim S, Brzozka K, Jung A, Kato H, Poeck H, Akira S, Conzelmann KK, Schlee M, Endres S, Hartmann G. 2006. 5′-Triphosphate RNA is the ligand for RIG-I. Science 314:994–997. https://doi.org/10.1126/science.1132505.
2. Kato H, Takeuchi O, Sato S, Yoneyama M, Yamamoto M, Matsui K, Uematsu S, Jung A, Kawai T, Ishii KJ, Yamaguchi O, Otsu K, Tsujimura T, Koh CS, Reis e Sousa C, Matsuura Y, Fujita T, Akira S. 2006. Differential roles of MDA5 and RIG-I helicases in the recognition of RNA viruses. Nature 441:101–105. https://doi.org/10.1038/nature04734.
3. Seth RB, Sun L, Ea CK, Chen ZJ. 2005. Identification and characterization of MAVS, a mitochondrial antiviral signaling protein that activates NF-κB and IRF 3. Cell 122:669–682. https://doi.org/10.1016/j.cell.2005.08.012.
4. Oganesyan G, Saha SK, Guo B, He JQ, Shahangian A, Zarnegar B, Perry A, Cheng G. 2006. Critical role of TRAF3 in the Toll-like receptor-dependent and -independent antiviral response. Nature 439:208–211. https://doi.org/10.1038/nature04374.
5. Zhao T, Yang L, Sun Q, Arguello M, Ballard DW, Hiscott J, Lin R. 2007. The NEMO adaptor bridges the nuclear factor-κB and interferon regulatory factor signaling pathways. Nat Immunol 8:592–600. https://doi.org/10.1038/ni1465.
6. Liu S, Chen J, Cai X, Wu J, Chen X, Wu YT, Sun L, Chen ZJ. 2013. MAVS recruits multiple ubiquitin E3 ligases to activate antiviral signaling cascades. eLife 2:e00785.
7. Fitzgerald KA, McWhirter SM, Faia KL, Rowe DC, Latz E, Golenbock DT, Coyle AJ, Liao SM, Maniatis T. 2003. IKKepsilon and TBK1 are essential components of the IRF3 signaling pathway. Nat Immunol 4:491–496. https://doi.org/10.1038/ni921.
8. Sharma S, ten Oever BR, Grandvaux N, Zhou GP, Lin R, Hiscott J. 2003. Triggering the interferon antiviral response through an IKK-related pathway. Science 300:1148–1151. https://doi.org/10.1126/science.1081315.
9. Chattopadhyay S, Marques JT, Yamashita M, Peters KL, Smith K, Desai A, Williams BR, Sen GC. 2010. Viral apoptosis is induced by IRF-3-mediated activation of Bax. EMBO J 29:1762–1773. https://doi.org/10.1038/emboj.2010.50.
10. Meylan E, Curran J, Hofmann K, Moradpour D, Binder M, Bartenschlager R, Tschopp J. 2005. Cardif is an adaptor protein in the RIG-I antiviral pathway and is targeted by hepatitis C virus. Nature 437:1167–1172. https://doi.org/10.1038/nature04193.
11. Lei Y, Moore CB, Liesman RM, O'Connor BP, Bergstralh DT, Chen ZJ, Pickles RJ, Ting JP. 2009. MAVS-mediated apoptosis and its inhibition by viral proteins. PLoS One 4:e5466. https://doi.org/10.1371/journal.pone.0005466.
12. Huang Y, Liu H, Li S, Tang Y, Wei B, Yu H, Wang C. 2014. MAVS-MKK7-JNK2 defines a novel apoptotic signaling pathway during viral infection. PLoS Pathog 10:e1004020. https://doi.org/10.1371/journal.ppat.1004020.
13. Michallet MC, Meylan E, Ermolaeva MA, Vazquez J, Rebsamen M, Curran J, Poeck H, Bscheider M, Hartmann G, Konig M, Kalinke U, Pasparakis M, Tschopp J. 2008. TRADD protein is an essential component of the RIG-like helicase antiviral pathway. Immunity 28:651–661. https://doi.org/10.1016/j.immuni.2008.03.013.
14. Balachandran S, Thomas E, Barber GN. 2004. A FADD-dependent innate immune mechanism in mammalian cells. Nature 432:401–405. https://doi.org/10.1038/nature03124.
15. El Maadidi S, Faletti L, Berg B, Wenzl C, Wieland K, Chen ZJ, Maurer U, Borner C. 2014. A novel mitochondrial MAVS/caspase-8 platform links RNA virus-induced innate antiviral signaling to Bax/Bak-independent apoptosis. J Immunol 192:1171–1183. https://doi.org/10.4049/jimmunol.1300842.
16. Guan K, Zheng Z, Song T, He X, Xu C, Zhang Y, Ma S, Wang Y, Xu Q, Cao Y, Li J, Yang X, Ge X, Wei C, Zhong H. 2013. MAVS regulates apoptotic cell death by decreasing K48-linked ubiquitination of voltage-dependent anion channel 1. Mol Cell Biol 33:3137–3149. https://doi.org/10.1128/MCB.00030-13.
17. Gachon F, Peleraux A, Thebault S, Dick J, Lemasson I, Devaux C, Mesnard JM. 1998. CREB-2, a cellular CRE-dependent transcription repressor, functions in association with Tax as an activator of the human T-cell leukemia virus type 1 promoter. J Virol 72:8332–8337.
18. De Valck D, Jin DY, Heyninck K, Van de Craen M, Contreras R, Fiers W, Jeang KT, Beyaert R. 1999. The zinc finger protein A20 interacts with a novel anti-apoptotic protein which is cleaved by specific caspases. Oncogene 18:4182–4190. https://doi.org/10.1038/sj.onc.1202787.
19. Ling L, Goeddel DV. 2000. T6BP, a TRAF6-interacting protein involved in IL-1 signaling. Proc Natl Acad Sci U S A 97:9567–9572. https://doi.org/10.1073/pnas.170279097.
20. Shembade N, Harhaj NS, Liebl DJ, Harhaj EW. 2007. Essential role for TAX1BP1 in the termination of TNF-alpha-, IL-1- and LPS-mediated NF-κB and JNK signaling. EMBO J 26:3910–3922. https://doi.org/10.1038/sj.emboj.7601823.
21. Iha H, Peloponese JM, Verstrepen L, Zapart G, Ikeda F, Smith CD, Starost MF, Yedavalli V, Heyninck K, Dikic I, Beyaert R, Jeang KT. 2008. Inflammatory cardiac valvulitis in TAX1BP1-deficient mice through selective NF-κB activation. EMBO J 27:629–641. https://doi.org/10.1038/emboj.2008.5.
22. Harhaj EW, Dixit VM. 2012. Regulation of NF-κB by deubiquitinases. Immunol Rev 246:107–124. https://doi.org/10.1111/j.1600-065X.2012.01100.x.
23. Shembade N, Harhaj NS, Parvatiyar K, Copeland NG, Jenkins NA, Matesic LE, Harhaj EW. 2008. The E3 ligase Itch negatively regulates inflammatory signaling pathways by controlling the function of the ubiquitin-editing enzyme A20. Nat Immunol 9:254–262. https://doi.org/10.1038/ni1563.
24. Shembade N, Parvatiyar K, Harhaj NS, Harhaj EW. 2009. The ubiquitin-editing enzyme A20 requires RNF11 to downregulate NF-κB signalling. EMBO J 28:513–522. https://doi.org/10.1038/emboj.2008.285.
25. Parvatiyar K, Barber GN, Harhaj EW. 2010. TAX1BP1 and A20 inhibit antiviral signaling by targeting TBK1-IKKi kinases. J Biol Chem 285:14999–15009. https://doi.org/10.1074/jbc.M110.109819.
26. Tumbarello DA, Manna PT, Allen M, Bycroft M, Arden SD, Kendrick-Jones J, Buss F. 2015. The autophagy receptor TAX1BP1 and the molecular motor myosin VI Are required for clearance of Salmonella Typhimurium by autophagy. PLoS Pathog 11:e1005174. https://doi.org/10.1371/journal.ppat.1005174.
27. Lazarou M, Sliter DA, Kane LA, Sarraf SA, Wang C, Burman JL, Sideris DP, Fogel AI, Youle RJ. 2015. The ubiquitin kinase PINK1 recruits autophagy receptors to induce mitophagy. Nature 524:309–314. https://doi.org/10.1038/nature14893.
28. Boulares AH, Yakovlev AG, Ivanova V, Stoica BA, Wang G, Iyer S, Smulson M. 1999. Role of poly(ADP-ribose) polymerase (PARP) cleavage in apoptosis. Caspase 3-resistant PARP mutant increases rates of apoptosis in transfected cells. J Biol Chem 274:22932–22940.
29. Balachandran S, Roberts PC, Kipperman T, Bhalla KN, Compans RW, Archer DR, Barber GN. 2000. Alpha/beta interferons potentiate virus-induced apoptosis through activation of the FADD/caspase-8 death signaling pathway. J Virol 74:1513–1523. https://doi.org/10.1128/JVI.74.3.1513-1523.2000.
30. Fernandez M, Porosnicu M, Markovic D, Barber GN. 2002. Genetically engineered vesicular stomatitis virus in gene therapy: application for treatment of malignant disease. J Virol 76:895–904. https://doi.org/10.1128/JVI.76.2.895-904.2002.
31. Zimmermann P, Bleuler S, Laule O, Martin F, Ivanov NV, Campanoni P, Oishi K, Lugon-Moulin N, Wyss M, Hruz T, Gruissem W. 2014. ExpressionData—a public resource of high quality curated datasets representing gene expression across anatomy, development and experimental conditions. BioData Min 7:18. https://doi.org/10.1186/1756-0381-7-18.
32. Hruz T, Laule O, Szabo G, Wessendorp F, Bleuler S, Oertle L, Widmayer P, Gruissem W, Zimmermann P. 2008. Genevestigator v3: a reference expression database for the meta-analysis of transcriptomes. Adv Bioinformatics 2008:420747. https://doi.org/10.1155/2008/420747.
33. Richter B, Sliter DA, Herhaus L, Stolz A, Wang C, Beli P, Zaffagnini G, Wild P, Martens S, Wagner SA, Youle RJ, Dikic I. 2016. Phosphorylation of OPTN by TBK1 enhances its binding to Ub chains and promotes selective autophagy of damaged mitochondria. Proc Natl Acad Sci U S A 113:4039–4044. https://doi.org/10.1073/pnas.1523926113.
34. Estornes Y, Toscano F, Virard F, Jacquemin G, Pierrot A, Vanbervliet B, Bonnin M, Lalaoui N, Mercier-Gouy P, Pacheco Y, Salaun B, Renno T, Micheau O, Lebecque S. 2012. dsRNA induces apoptosis through an atypical death complex associating TLR3 to caspase-8. Cell Death Differ 19:1482–1494. https://doi.org/10.1038/cdd.2012.22.
35. Hwang KY, Choi YB. 2015. Modulation of mitochondrial antiviral signaling by human herpesvirus 8 interferon regulatory factor 1. J Virol 90:506–520. https://doi.org/10.1128/JVI.01903-15.
36. Brubaker SW, Gauthier AE, Mills EW, Ingolia NT, Kagan JC. 2014. A bicistronic MAVS transcript highlights a class of truncated variants in antiviral immunity. Cell 156:800–811. https://doi.org/10.1016/j.cell.2014.01.021.

37. Yu CY, Chiang RL, Chang TH, Liao CL, Lin YL. 2010. The interferon stimulator mitochondrial antiviral signaling protein facilitates cell death by disrupting the mitochondrial membrane potential and by activating caspases. J Virol 84:2421–2431. https://doi.org/10.1128/JVI.02174-09.
38. Vazquez C, Horner SM. 2015. MAVS coordination of antiviral innate immunity. J Virol 89:6974–6977. https://doi.org/10.1128/JVI.01918-14.
39. Castanier C, Zemirli N, Portier A, Garcin D, Bidere N, Vazquez A, Arnoult D. 2012. MAVS ubiquitination by the E3 ligase TRIM25 and degradation by the proteasome is involved in type I interferon production after activation of the antiviral RIG-I-like receptors. BMC Biol 10:44. https://doi.org/10.1186/1741-7007-10-44.
40. You F, Sun H, Zhou X, Sun W, Liang S, Zhai Z, Jiang Z. 2009. PCBP2 mediates degradation of the adaptor MAVS via the HECT ubiquitin ligase AIP4. Nat Immunol 10:1300–1308. https://doi.org/10.1038/ni.1815.
41. Zhou X, You F, Chen H, Jiang Z. 2012. Poly(C)-binding protein 1 (PCBP1) mediates housekeeping degradation of mitochondrial antiviral signaling (MAVS). Cell Res 22:717–727. https://doi.org/10.1038/cr.2011.184.
42. Fujimura K, Katahira J, Kano F, Yoneda Y, Murata M. 2009. Selective localization of PCBP2 to cytoplasmic processing bodies. Biochim Biophys Acta 1793:878–887. https://doi.org/10.1016/j.bbamcr.2009.02.002.
43. Yoo YS, Park YY, Kim JH, Cho H, Kim SH, Lee HS, Kim TH, Sun Kim Y, Lee Y, Kim CJ, Jung JU, Lee JS, Cho H. 2015. The mitochondrial ubiquitin ligase MARCH5 resolves MAVS aggregates during antiviral signalling. Nat Commun 6:7910. https://doi.org/10.1038/ncomms8910.
44. Wang Y, Tong X, Ye X. 2012. Ndfip1 negatively regulates RIG-I-dependent immune signaling by enhancing E3 ligase Smurf1-mediated MAVS degradation. J Immunol 189:5304–5313. https://doi.org/10.4049/jimmunol.1201445.
45. Zhong B, Zhang Y, Tan B, Liu TT, Wang YY, Shu HB. 2010. The E3 ubiquitin ligase RNF5 targets virus-induced signaling adaptor for ubiquitination and degradation. J Immunol 184:6249–6255. https://doi.org/10.4049/jimmunol.0903748.
46. Jacobs JL, Zhu J, Sarkar SN, Coyne CB. 2014. Regulation of mitochondrial antiviral signaling (MAVS) expression and signaling by the mitochondria-associated endoplasmic reticulum membrane (MAM) protein Gp78. J Biol Chem 289:1604–1616. https://doi.org/10.1074/jbc.M113.520254.
47. Pan Y, Li R, Meng JL, Mao HT, Zhang Y, Zhang J. 2014. Smurf2 negatively modulates RIG-I-dependent antiviral response by targeting VISA/MAVS for ubiquitination and degradation. J Immunol 192:4758–4764. https://doi.org/10.4049/jimmunol.1302632.
48. Du J, Zhang D, Zhang W, Ouyang G, Wang J, Liu X, Li S, Ji W, Liu W, Xiao W. 2015. pVHL negatively regulates antiviral signaling by targeting MAVS for proteasomal degradation. J Immunol 195:1782–1790. https://doi.org/10.4049/jimmunol.1500588.
49. Wang X, Naidu SR, Sverdrup F, Androphy EJ. 2009. Tax1BP1 interacts with papillomavirus E2 and regulates E2-dependent transcription and stability. J Virol 83:2274–2284. https://doi.org/10.1128/JVI.01791-08.
50. Shembade N, Pujari R, Harhaj NS, Abbott DW, Harhaj EW. 2011. The kinase IKKα inhibits activation of the transcription factor NF-κB by phosphorylating the regulatory molecule TAX1BP1. Nat Immunol 12:834–843. https://doi.org/10.1038/ni.2066.
51. Choi YB, Harhaj EW. 2014. HTLV-1 tax stabilizes MCL-1 via TRAF6-dependent K63-linked polyubiquitination to promote cell survival and transformation. PLoS Pathog 10:e1004458. https://doi.org/10.1371/journal.ppat.1004458.
52. Shembade N, Ma A, Harhaj EW. 2010. Inhibition of NF-κB signaling by A20 through disruption of ubiquitin enzyme complexes. Science 327:1135–1139. https://doi.org/10.1126/science.1182364.
53. Schneider CA, Rasband WS, Eliceiri KW. 2012. NIH Image to ImageJ: 25 years of image analysis. Nature Methods 9:671–675. https://doi.org/10.1038/nmeth.2089.
54. Liao H, Liu XJ, Blank JL, Bouck DC, Bernard H, Garcia K, Lightcap ES. 2011. Quantitative proteomic analysis of cellular protein modulation upon inhibition of the NEDD8-activating enzyme by MLN4924. Mol Cell Proteomics 10:M111.009183. https://doi.org/10.1074/mcp.M111.009183.